Available online at www.sciencedirect.com

ScienceDirect

MATTER AND RADIATION AT EXTREMES

Matter and Radiation at Extremes 3 (2018) 312–321

www.journals.elsevier.com/matter-and-radiation-at-extremes

Research Article

Properties of vapor-deposited and solution-processed targets for laser-driven inertial confinement fusion experiments

D.R. Harding [a,b,*], M.J. Bonino [a], W. Sweet [c], M. Schoff [c], A. Greenwood [c], N. Satoh [d], M. Takagi [e], A. Nikroo [f]

[a] *Laboratory for Laser Energetics, University of Rochester, 250 East River Road, Rochester, NY 14623-1299, USA*
[b] *Department of Chemical Engineering, University of Rochester, Rochester, NY 14623-1299, USA*
[c] *General Atomics, 3550 General Atomics Court, San Diego, CA 92121-1122, USA*
[d] *Industrial Development Center, Central Research Laboratory, Hamamatsu Photonics K.K., Hamamatsu City, Shizuoka Pref., 431-1202, Japan*
[e] *Institute of Laser Engineering, Osaka University, 2–6 Yamadaoka, Suita, Osaka 565-0871, Japan*
[f] *Lawrence Livermore National Laboratory, P.O. Box 808, Livermore, CA, 94550, USA*

Received 8 May 2018; revised 1 August 2018; accepted 29 August 2018
Available online 21 October 2018

Abstract

Targets for low-adiabat direct-drive-implosion experiments on OMEGA must meet rigorous specifications and tight tolerances on the diameter, wall thickness, wall-thickness uniformity, and presence of surface features. Of these, restrictions on the size and number of defects (bumps and depressions) on the surface are the most challenging. The properties of targets that are made using vapor-deposition and solution-based microencapsulation techniques are reviewed.

Targets were characterized using confocal microscopy, bright- and dark-field microscopy, atomic force microscopy, electron microscopy, and interferometry. Each technique has merits and limitations, and a combination of these techniques is necessary to adequately characterize a target.

The main limitation with the glow-discharge polymerization (GDP) method for making targets is that it produces hundreds of domes with a lateral dimension of 0.7–2 μm. Polishing these targets reduces the size of some but not all domes, but it adds scratches and grooves to the surface. Solution-made polystyrene shells lack the dome features of GDP targets but have hundreds of submicrometer-size voids throughout the wall of the target; a few of these voids can be as large as ~12 μm at the surface.

PACS Codes: 82.35.-x; 52.57.Bc; 07.79.-v

Keywords: Vapor-deposition; Direct-drive target; OMEGA; Target characterization; Solution-based microencapsulation

1. Introduction

Millimeter-size plastic shells are used as targets for implosion physics experiments at the Laboratory for Laser Energetics (LLE) and the National Ignition Facility (NIF) (see Fig. 1). Targets for the experiments on OMEGA are typically 0.86 mm in diameter with an 8- to 27-μm-thick wall and are filled with a mixture of deuterium and tritium (DT). A subset of these shells (those with an 8-μm-thick wall) are filled to high gas densities (~0.1 g/cm^3), then cooled to 19.6 K to form a shell of DT ice inside the plastic shell that can be up to 100 μm thick. Implosions of these targets have produced up to 5×10^{13} neutrons, a pressure of 56 Gbar in the core of the implosion, and areal densities up to 240 mg/cm^2 [1]. An

* Corresponding author. Laboratory for Laser Energetics, University of Rochester, 250 East River Road, Rochester, NY 14623-1299, USA.
E-mail address: dhar@lle.rochester.edu (D.R. Harding).
Peer review under responsibility of Science and Technology Information Center, China Academy of Engineering Physics.

https://doi.org/10.1016/j.mre.2018.08.001

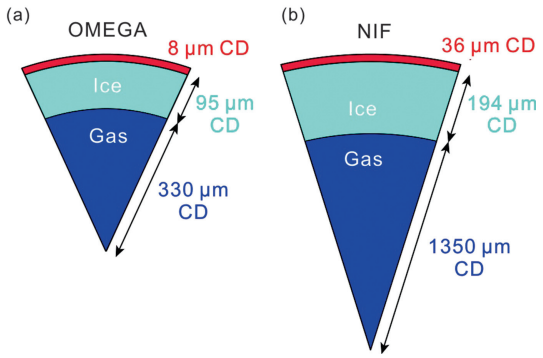

Fig. 1. Schematic of the plastic shells containing DT ice for experiments on (a) OMEGA and (b) the National Ignition Facility (NIF).

internal goal is to increase the core pressure to 100 Gbar, a value that scales to near ignition with MJ energy at the NIF [2]. Achieving this goal requires a smooth target with few defects on the surface, which can perturb the implosion. This paper describes a thorough characterization of targets made by using two different processing techniques to quantify the type and number of defects and to identify other criteria that are important such as control of the target's diameter, wall thickness, and wall-thickness uniformity.

Features on the surface must be as small and few as possible. Features represent a variation in mass at the ablation surface (whether they are a dome or a depression), which affects the local velocity of the surface; since the implosion is hydrodynamically unstable, this perturbation grows as the target implodes. The effect of this perturbation on the imploded core pressure and yield depends on the height and lateral dimension of the features; simulations and modeling show that those features with lateral dimensions of 0.7–2 μm have the most-restrictive height constraint [3]. The length of all features above the curve is summed in quadrature, and the target is rejected if the resulting area is more than 100 μm^2. (The curve is presented together with the results from a target in Section 3.)

Plastic shells are made using two different processes: glow-discharge polymerization (GDP), which is a vapor-phase process [4], and microencapsulation [5]. The first method deposits a highly cross-linked polymer on a depolymerizable mandrel which is subsequently removed thermally. This method has been used to make shells for the Inertial Confinement Fusion (ICF) Program for decades. The advantages of this method are that the thickness of the shell wall can be precisely controlled (to within ±0.3 μm, the measurement accuracy) and dopants can be added to the polymer. The disadvantage is that shallow "dome-shaped" features resulting from the growth mechanism are common [4].

The second method uses a microfluidic solvent process to encapsulate an organic liquid (a polymer dissolved in a solvent) between two immiscible liquids to form a doubly encapsulated droplet [5]. This technique was used in the early 1990s to make plastic shells for the ICF Program, but more recently has been used to make the depolymerizable mandrels onto which the GDP material is coated. The advantage of this method is that the interfacial surface tension between the immiscible fluids smooths the surface, which is not possible with vapor-deposited films. A limitation of this method is that voids form in the polymer wall during the solvent-extraction process, which is used to form the solid plastic shell; those voids near the surface can form a blister or can erupt to form a depression. The polystyrene shells evaluated in this study were provided by General Atomics and Hamamatsu Photonics K.K.

2. Experimental setup and instrumentation

The shells' outer diameters and wall thicknesses were measured using a compound microscope and white-light interferometer. This microscope has a long-working-distance Mitutoyo optic (M Plan Apo SL 50×, 0.42 N.A., 2× variable magnifier) and a Heidenheim Quadracheck digital readout for the *x*- and *y*-translation stages which was used in both transmitted and reflected white-light modes. Images were captured using an Imperx CCD IXP-4M15 camera. The shells' diameters were determined from the position in the image between the first bright and dark diffractive fringes using transmitted light and a 50× objective lens; the translation-stage encoders have a precision of 0.1 μm. The measurement accuracy of this equipment was calibrated to be 1 μm using a NIST (National Institute for Standards and Technology) traceable sapphire bead. Nine measurements around the circumference were acquired and fit to a circle using a least-mean-square method. The circle fit is reported as the shell diameter.

The wall thickness was measured using a Leica DCM 3-D confocal microscope with a 150× objective lens, 0.95 N.A., 460-nm LED illumination, and a material index of refraction of 1.611. The thickness was measured at 90° increments along one great circle of the shell.

A separate measurement of the wall thickness was made using a Filmetrics interferometer (model FZO) with nanometer resolution. The shell was rotated about the vertical axis and the interferometer calculated the wall thickness as a function of the angle using the index of refraction of each medium (air, polystyrene, air) and Filmetrics software. The shell was repositioned and remeasured twice along orthogonal great circles to obtain a low-mode 3-D map of the thickness variation. The greatest variation among the three measurements is reported as the shell's "delta wall."

Features larger than 5 μm (footprint) on the surface of the shells were characterized using a compound microscope with Mitutoyo optic (M Plan Apo SL 5× magnification, 0.14 N.A.). Smaller features, down to the detection limit of 1 μm (footprint), were identified using a 100× Mitutoyo objective lens and Imperx camera (M Plan Apo SL 100×, 0.55 N.A., 75-μm × 75-μm field of view, 1.6-μm depth of field). The dimensions of these features were measured using calibrated *x*- and *y*-translation stages (0.1-μm precision).

The height was measured and a more-accurate spatial measurement of all features was made using an atomic force microscope (AFM, NanoSurf Lens). The equipment has a noise floor of ±2 nm, and the accuracy of the height

measurement is ~10 nm. The spatial accuracy of the measurement was determined by the size (<10 nm) and conical shape of the probe's tip. One limitation to this technique is the time required to scan the surface; an 82-μm × 82-μm area requires 4 h to characterize at a linear scan rate of 15 μm/s, which extrapolates to 22 days for an OMEGA target. Using a faster linear scan rate of 40 μm/s increased the noise floor to ±10-nm rms and distorted the shape of the larger features (<1-μm lateral dimension).

Confocal microscopy (Leica DCM 3-D microscope using a 150× objective lens, 0.95 N.A) can characterize the entire surface of an OMEGA target in less than a day (if automated) but at a lower spatial resolution: the equipment can resolve ~0.3-μm features (footprint) without simultaneously acquiring height information or 0.8-μm features with 10-nm height resolution. One advantage of the confocal microscope is that it can operate as a dark-field microscope: Features are illuminated using scattered light rather than standard bright-field illumination, which improves the detection threshold. Detectability depends on the contrast, which depends on the geometry of the feature [6].

The dark-field capability is especially valuable for identifying spherical voids inside the shell's wall. The confocal microscope scanned in 0.5-μm vertical increments (with 10-nm vertical resolution and 0.8-μm lateral resolution) through the shell's wall to identify scattering sites. The depth-of-focus for this equipment is very narrow (<0.5 μm), so features are in focus only at specific depths within the wall. Larger voids appear as defocused features at different depth positions, so multiple images at different depths of the same area of the shells are compared to form a 3-D map of the void structure inside the shell's wall. The images were processed using Mountains and ImageJ software [7,8].

Scanning electron microscope (SEM) images were acquired with two Zeiss field emission microscopes operating at low electron energies (<2 keV): one was an Auriga crossbeam (FIB-SEM) workstation and the other was a Sigma HD VP microscope, each of which provided improved sensitivity to identify surface features than SEMs (scanning electron microscopes) equipped with LaB_6 or tungsten electron sources. The Sigma HD microscope operates in a variable pressure mode that allows the surface of shells to be imaged without adding a metallic overcoat to prevent the surface from charging.

3. Results and discussion

3.1. Shell dimensions

The capability of the GDP process to produce shells with precisely controlled dimensions has been well established and needs no further elaboration [9]. Conversely, the capability to manufacture polystyrene shells using a focused-flow microfluidic device is new to the ICF program in the U.S., so the diameters, wall thicknesses, nonconcentricities, and "out of roundness" (OOR) of 30 shells made by Hamamatsu photonics K.K. are summarized. These values are 874.5 ± 0.9 μm, 9.00 ± 0.13 μm, 2.04, and 0.1, respectively, for a sample of shells taken from a single production batch. The OOR was calculated from multiple diameter measurements of a single target acquired at different orientations and expressed as the percentage difference between the largest value and the average of all the values ((maximum diameter−average diameter) × 100%/average diameter). The nonconcentricity is calculated from multiple wall-thickness measurements of a single target acquired at different orientations and expressed as the percentage difference between the largest value and the average of all the values ((largest wall thickness − average wall thickness) × 100%/average wall thickness).

The variation in the thickness of the wall of a single polystyrene shell (supplied by Hamamatsu Photonics K.K.) ranged from 0.9% to 5.6% (Fig. 2(a)), which is greater than the average variation of the shells' wall for a single production batch of targets. The wall thickness measurement is cross referenced with a second measurement technique that uses the Filmetrics™ wall-mapper unit. Three shells, taken from the

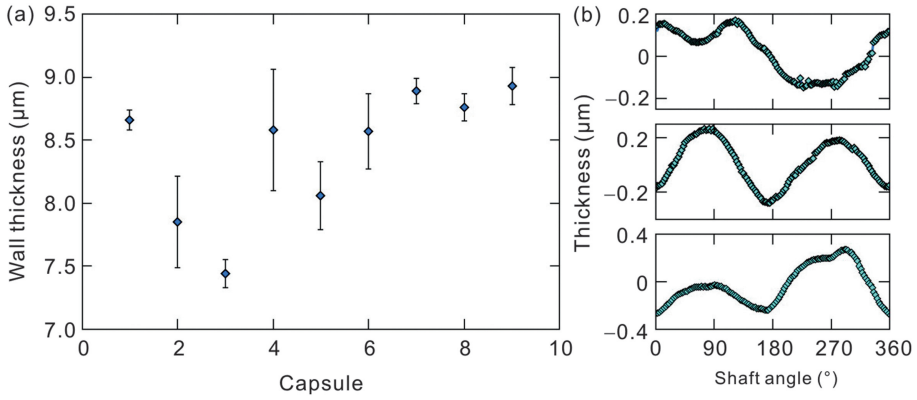

Fig. 2. (a). The wall thickness of ten polystyrene targets was measured at 90° increments along one great circle of the shell using confocal microscopy. (b) The variation in the thickness of the wall of one polystyrene target (9 μm thick; 0.54 μm peak-valley) was measured along three orthogonal great circles using interferometry.

same production batch of shells, had a maximum thickness variation of 0.54 μm, 0.32 μm, and 0.36 μm; the data for three orthogonal great circles around the shell with the greatest variation is shown in Fig. 2(b). The goal is to limit the thickness variation to less than 0.1 μm, so further refinement of the centering process [4,9] for making shells is needed to produce targets that meet the direct-drive specification.

3.2. Defects on the surface and within the wall of the shell

3.2.1. GDP targets

A 400-μm × 200-μm region of the surface of two shells (3.5% of the total surface) was imaged using electron microscopy (Fig. 3). These areas contained approximately 120 and 200 dome-like features (approximately shaped like a spherical cap), respectively, with a footprint smaller than 5-μm diameter. Scaling this number proportionally to the total surface area suggests that 3000–5000 features are presented on the shells. Importantly, these features were not stochastically distributed; many of these features were domes that were clustered near to each other—a configuration where their combined presence will affect the implosion much more than if they were more distantly distributed.

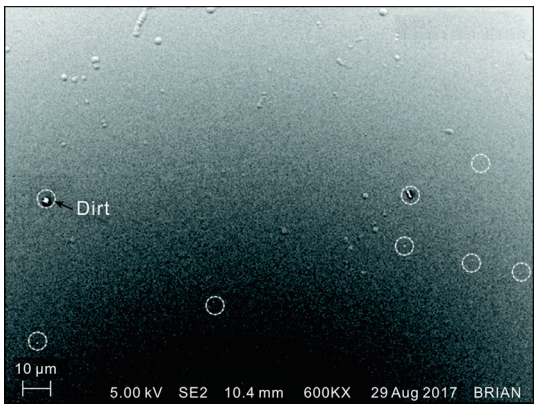

Fig. 3. Domes and dirt are seen in an electron micrograph image of a 180-μm × 130-μm region of a typical target used for cryogenic implosion experiments. The domes are smaller than 5 μm, and many of them are clustered closely together. The dirt pieces are circled and presented in two sizes: two pieces are 2–3 μm and six pieces are smaller than 1 μm. The larger pieces that are loosely attached to the surface are more readily charged by the electron beam and appear to be brighter.

Domes were observed on the inner surface of the shell that was fractured to allow the surface to be inspected (Fig. 4(a)–(b)). These domes are presumed to result from depressions in the plastic mandrel that were filled with GDP during the vapor-deposition process and were left projecting from the surface when the mandrel was removed. (The depressions in the mandrel are attributed to vacuoles in the poly-α-methylstyrene mandrel). Additionally, a nodule (<0.5-μm diameter), which would be a dome at the surface, and a void (~1 μm) were observed inside the wall of the shell (Fig. 5(a)–(b)). The nodular shape of the features was unexpected since domes were presumed to grow in width with increasing wall thickness and did not self-terminate, which was what these features did [10]. The smooth shape of the nodules suggested that the shell fractured around the boundary of the nodules rather than through them, and that the nodules were a natural part of the shell wall and not an artifact of the fracture process. Elliptically shaped features like this have not been reported previously, but conically shaped features in the wall of the GDP shell were reported when the GDP process was first developed and were believed now to be absent [10]. These features were observed only in the target that was fractured for this study, so no comment can be made about their prevalence. Such statement will require multiple targets to be prepared following a standard metallographic method (ASTM E2015-04(2014) protocol "Standard Guide for Preparation of Plastics and Polymeric Specimens for Microstructural Examination") and analyzed.

The void in the wall was presumed to result from the fracturing process that caused a portion of the shell wall to delaminate and detach; this feature was more an indication of a flaw in the structural integrity of the wall than the presence of a void in an unfractured wall.

One shell imaged with the SEM was also imaged with the confocal and atomic force microscopes (Figs. 6 and 7). The height and base dimensions of the domes with a footprint larger than 1 μm, as measured by each technique, were in good

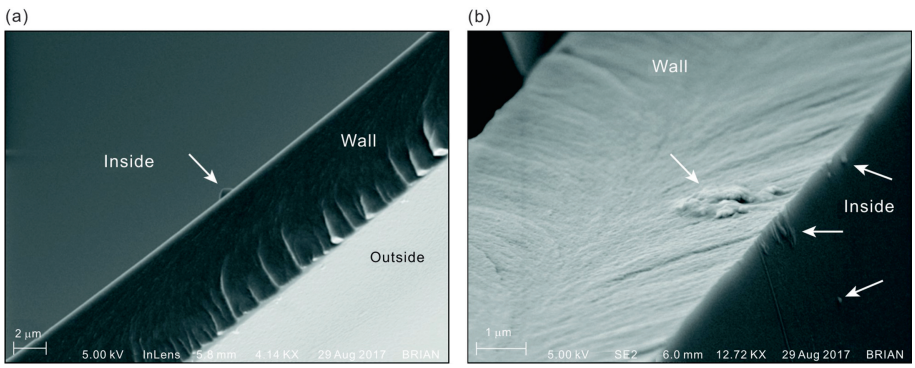

Fig. 4. Electron micrograph images of the wall and inner surface of a fractured target show (a) a dome-like structure ~0.6 μm wide and ~0.2 μm high on the inner surface (see the arrow in center of the image). (b) Very small domes are visible in the wall and on the inner surface. The inner and outside surfaces are indicated.

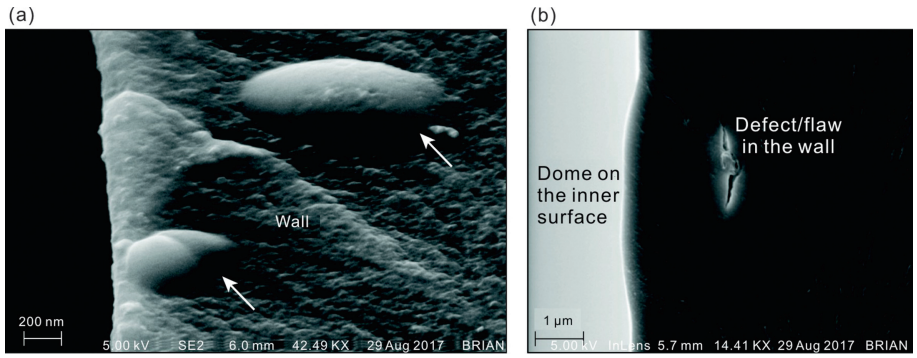

Fig. 5. A highly magnified image of the wall of a fractured target shows (a) two dome-like nodular structures within the wall and close to the inner surface of the target, and (b) a shallow dome/bulge on the inner surface and a 1-µm-long crack inside the wall. The crack is parallel to the surface and ~1.5 µm away from the inner surface.

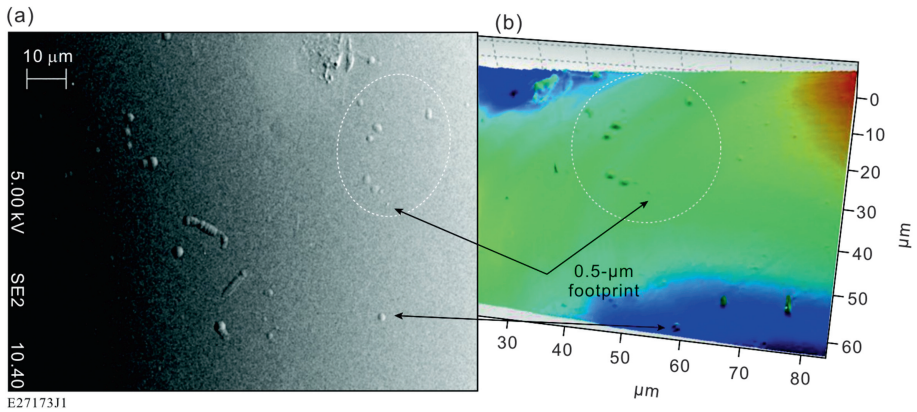

Fig. 6. (a) An electron micrograph and (b) a confocal microscopic image of the same region of a target which are rotated to a position where features common to both images can be more easily correlated. The circled region shows a cluster of features common to both images.

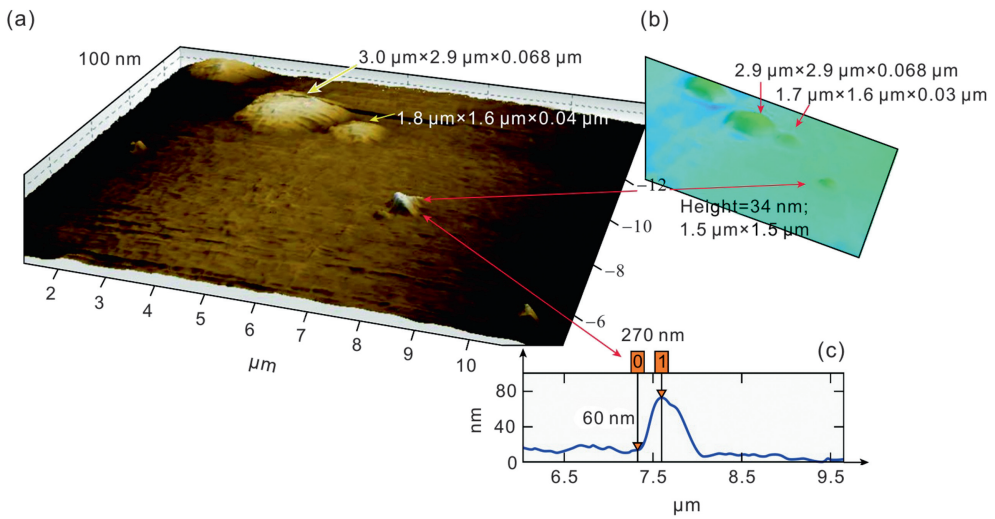

Fig. 7. A region of the surface of a target that was imaged by both AFM and confocal microscope, which is rotated to align the features in each image. The height and base dimensions of the features as measured by each technique are annotated on the respective images. A lineout profile through one submicrometer feature in the AFM image is inset: this feature has a smaller footprint and is higher than what the confocal measurement shows.

agreement. Small domes (<1 μm) were slightly larger when measured using confocal microscopy than when measured using AFM; the shape of these domes was more peaked (larger height-to-base aspect ratio) when measured using AFM than when measured using confocal microscopy. In this size range, the AFM-measured value provides a more-accurate representation of the shape of the feature.

The surface of seven shells intended for implosion experiments was analyzed using bright-field microscopy. An example of the images is shown in Fig. 8. Features closest to the center of the image where the microscope was focused appear as discrete black dots; features farther removed from the center are increasingly out of focus and appear as rings—a consequence of the curvature of the shell's surface and the narrow depth of field of the microscope objective. The size of the features ranged from the detection threshold (<1 μm) to ~10 μm. The observed features are either on the surface or in the wall of the shell: the depth-of-field for the objective is 1.6 μm. No out-of-focus features were observed in the center of the images, which would be expected if the features were on the inner surface of the shell's wall. Focusing down through the shell's surface brings the features on the perimeter of the image into focus. (The curvature of the shell places the object plane at the perimeter of the image 5.7 μm below the object plane for the center of the image, well out of the depth-of-focus for the microscope objective.)

The number of features in each image, and for each shell, is shown in Fig. 9. The total number of features on each shell is 131, 126, 434, 253, 119, 518, and 538. These numbers are for an area that is 16% of the total area. Extrapolating the number of features to the total surface area of the shell gives numbers of 793, 762, 2626, 1531, 715, 3291, and 3483. The uncertainty in extrapolating the observed numbers to represent the total surface cannot be quantified; to do so will require the entire surface of a statistically significant number of targets be fully characterized so that the number of defects in differently sized smaller areas, that are randomly distributed over the surface of the target, can be assessed. This task is beyond the scope of the current work, but is planned for future studies.

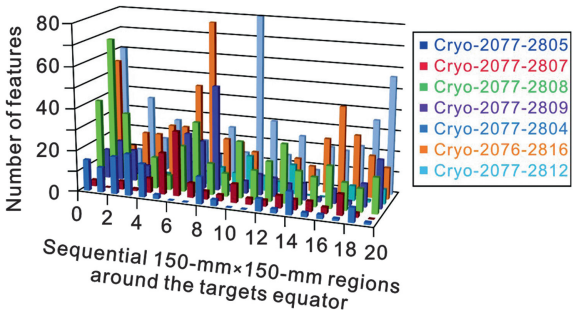

Fig. 9. The number and distribution of features in adjoining 150-μm × 150-μm areas around the equator of seven targets which are randomly distributed.

3.2.2. GDP targets

Targets for X-ray-driven-implosion experiments at the NIF are polished to reduce the height of features (domes) that are typically much larger in those thick-wall shells than they are in direct-drive targets [9]. The same polishing protocol that is used for the NIF targets was used to polish the OMEGA-size targets. This protocol is proprietary to General Atomics and Lawrence Livermore National Laboratories and is not discussed here. The results are shown in Figs. 10–13. In general, polishing reduces the height of some of the domes; however, this process can form a groove around the perimeter of the dome (Fig. 10). Polishing does not remove all the domes on the surface (Figs. 11 and 12), and there are instances where artifacts such as grooves and scratches are added to the surface

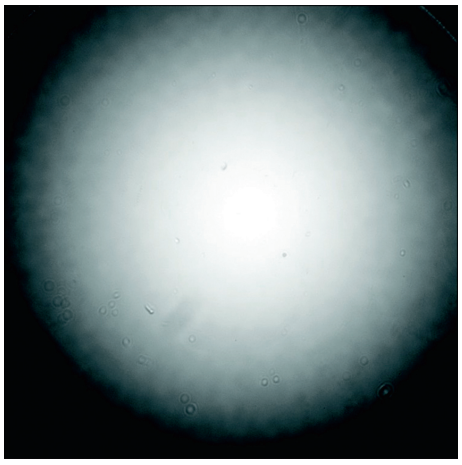

Fig. 8. A bright-field microscope image of the surface of an implosion target shows micrometer-size features on the surface. This technique has been the standard method for characterizing targets until now when features smaller than the detection threshold and resolution of white-light microscopy need to be quantified. The area of the image is 150 μm × 150 μm (100× magnification). Features outside the center of the image appear circular and are out of focus.

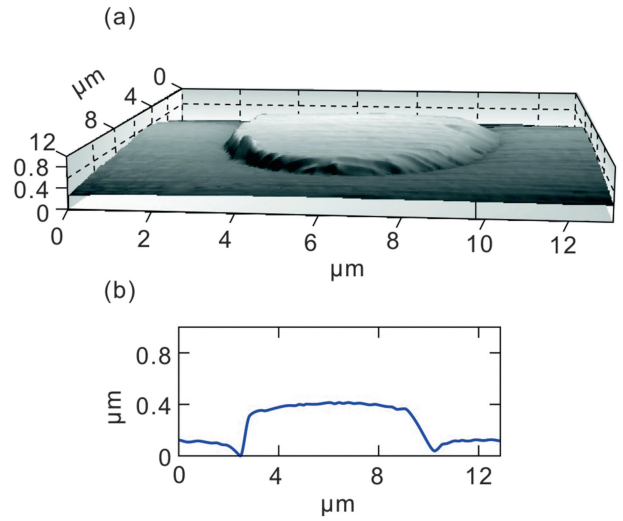

Fig. 10. (a) An AFM 3-D profile of the shape and size of a dome on a polished target. The typical dome-like structure of the feature is truncated by the polishing process. (b) A 1-D lineout across the dome shows the presence of a ~0.1-μm groove around the perimeter of the dome that was formed by the entrapped polishing medium.

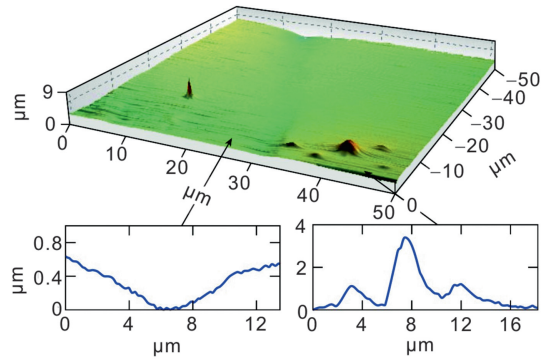

Fig. 11. An AFM 3-D profile of a 50-μm × 50-μm area of a polished target shows the presence of an ~0.8-μm groove running across the surface of the target and a cluster of domes up to 3.5 μm high and with a base of ~14 μm. The inset 1-D profiles show the height and length of the groove and dome cluster.

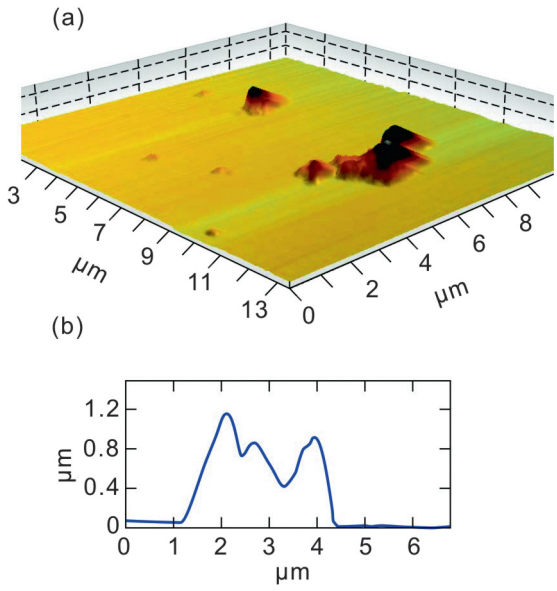

Fig. 12. A high-resolution AFM 3-D profile of a 13-μm × 13-μm area of a polished target shows the size and shape of domes on the surface that do not appear to have been affected by the polishing process. A 1-D lineout through the cluster of domes shows the height and base dimensions.

by the polishing process (Figs. 11 and 13(a)). One of the features on the surface was analyzed using the electron dispersive analysis feature of the SEM and was shown to contain only carbon and oxygen atoms, proving in this case that the feature is not the polishing media or a particulate from the environment (Fig. 13(b)).

A compilation of the number and size of defects on an area of 0.031 mm^2 (1.3% of the total area) on a single shell, as measured by AFM, is shown in Fig. 14. These data are superimposed over the acceptance profile [3] and show that a majority of the features fall above the acceptance threshold. A similar analysis of polystyrene shell (discussed below) is shown in Fig. 14(b).

3.2.3. Polystyrene shells

Defects in polystyrene shells differ from those in GDP shells because of the different surface-energy forces and solubility parameters that control the liquid-based microencapsulation process. Surface tension provides a flat interface between two immiscible liquids that prevents domes from forming. However, the slight mutual solubility of the nominally immiscible liquids that are used to make the double emulsion (which is the liquid precursor to the solid shell) results in vacuoles forming inside the shell's wall. These vacuoles become voids when the liquids are extracted to form the solid shell, and the dissolved secondary-liquid phase separates into discrete submicrometer-size liquid-filled spheres (vacuoles) [11]. Those vacuoles near the surface may burst during the solvent-extraction process and form depressions (Fig. 15), while others may create a bulge in the surface that appears to be "dome-like." Other mechanisms in the manufacturing process can compromise the smoothness of the polystyrene shells—primarily the shell cracking while drying; however, these features are large (over 100 μm in diameter) and the shells are easily identified and eliminated, thus they do not require the same level of detailed characterization.

Polystyrene targets were characterized using electron, confocal, dark-field, and atomic force microscopy to measure the shape and size of the surface and subsurface features. Ten of the 14 shells had depressions in the surface that were

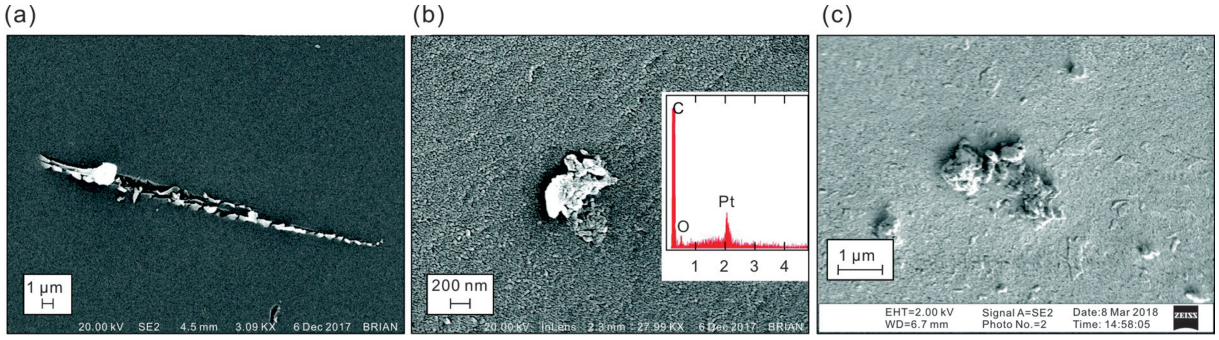

Fig. 13. Scanning electron microscope images of the surface of two polished glow-discharge polymerization (GDP) targets. (a) Scratches longer than 10 μm are from the polishing media grinding into the surface. (b) Dirt on the surface is smaller than 1 μm and is composed of only carbon and oxygen. The energy dispersive X-ray spectrum of the "dirt" particle is inset (the Pt signal is from the ~50-nm-thick charge-dissipating metallic overcoat). (c) The surface of a polished target has no charge-dissipating metallic overcoat.

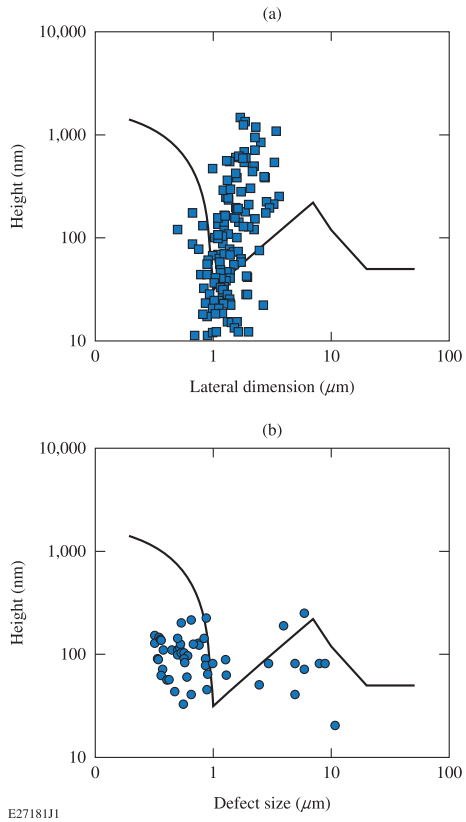

Fig. 14. The dimensions (height and lateral) of the features on: (a) a 0.031-mm^2 area (1.3% of total area) of a polished GDP target and (b) a 0.065-mm^2 area (2.8% of total area) of a polystyrene shell, are shown superimposed over the acceptance curve [3]. Approximately 1% of the area of the GDP shell analyzed does not meet the OMEGA specification, while 0.04% of the area of the polystyrene shell analyzed does not meet the OMEGA specification.

derived from burst vacuoles. Seven shells were imaged using confocal microscopy at four random locations along a great circle: an area of 0.005 mm^2 (0.2% of the total surface area) contained an average of 15 dome-like defects (averaging

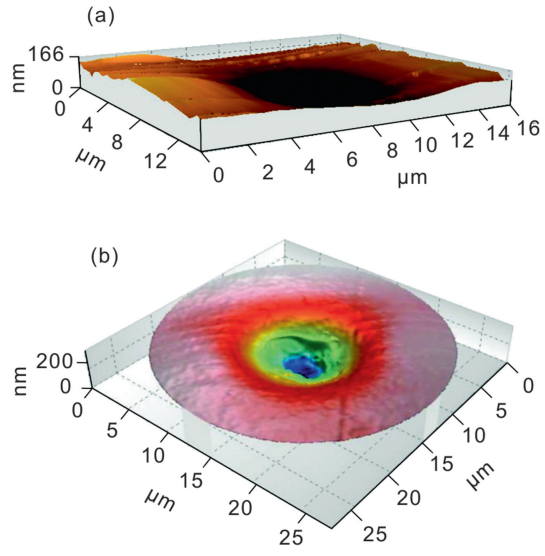

Fig. 15. (a) Atomic force and (b) confocal microscopic images of the same depression in the surface of a polystyrene shell.

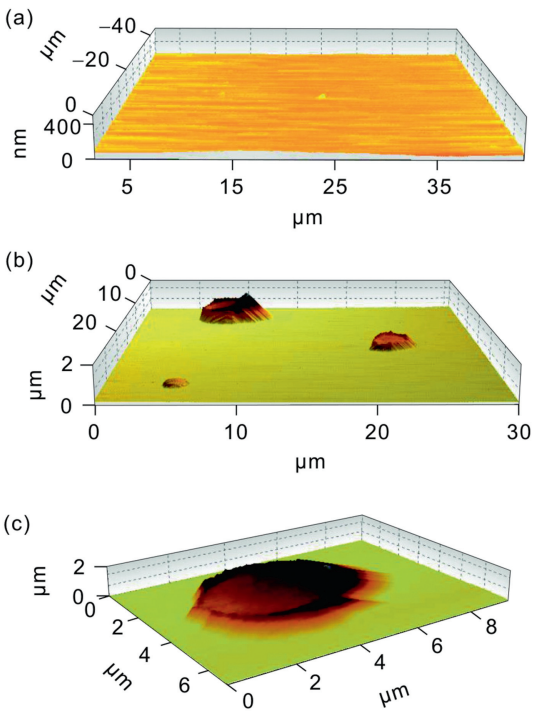

Fig. 16. AFM scans of different regions of the surface of a polystyrene shell: (a) a 44-nm × 0.9-μm (height versus lateral dimension) dome in an otherwise smooth surface; (b) larger dome-like features, attributed to subsurface voids, with dimensions of 0.31 μm (diameter) × 1.9 μm, 3.1 μm × 4.1 μm × 0.49 μm, and 6.0 μm × 4.9 μm × 1.2 μm; (c) the largest feature in (b) with a crater-like depression in the center.

1.5 μm in diameter and 48 nm in height) and two depressions (4 μm in diameter and 0.4 μm in height; 0.3 μm in diameter and 0.5 μm in height, respectively). The domes were too shallow to exceed the acceptance threshold, but the depressions were unacceptable [3]. An additional shell was imaged around a great circle (~7% of the total surface area) and had 13 defects between 1 and 2 μm (lateral dimension) and no defects smaller than 1 μm; the diameter-to-height ratio was ~10:1.

Shells provided by General Atomics were imaged using the AFM. Areas ranging from 100 to 3000-μm^2 were scanned at linear rates up to 15 μm/s and required 1.5 h to completely characterize, a rate that if extrapolated to characterizing an entire target would require several months to complete. As a result, only features observed with bright-field microscopy were measured with the AFM. These surfaces were mostly very smooth (Fig. 16(a)); however, a few domed structures ranging in size from <1 μm × 0.1 μm (lateral × height) up to ~6 μm × 1.2 μm were present (Fig. 16(b)). These features were presumed to be caused by unruptured vacuoles just beneath the surface of the shell. The largest of the dome features, shown at higher resolution (Fig. 16(c)) possessed a crater-like depression in the middle of the dome, which is difficult to explain by any physical model. A SEM analysis of other shells revealed a mostly featureless surface containing domes smaller than 0.1 μm (Fig. 17(a)), scratches, tiny dirt particles (Fig. 17(b)), and larger dirt particles (Fig. 17(c)).

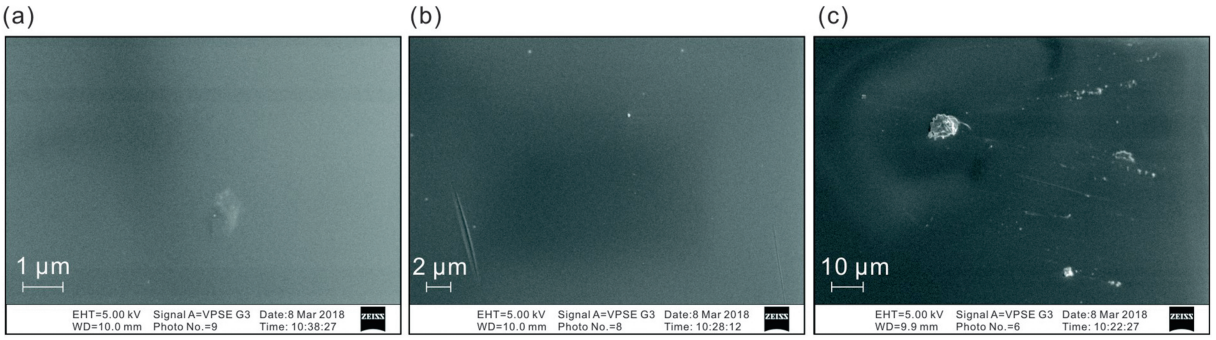

Fig. 17. Electron micrographs of the surface of a polystyrene shell acquired without any metallic coating show (a) a swelling from a subsurface void; (b) a scratch and tiny (<0.2 μm) dirt particulates; and (c) larger (5 μm) dirt particles.

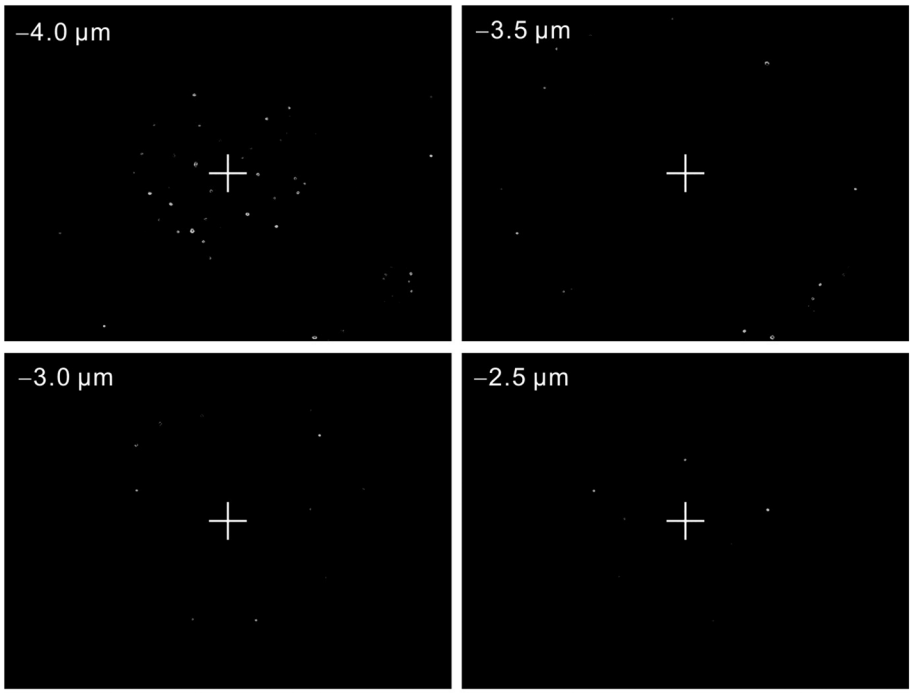

Fig. 18. Dark-field images of the wall of a polystyrene target. The field of view of each image is 85 μm × 64 μm. Each image is in focus at discrete depths within the wall of the target; the indicated values are the distance from the top surface of the target. Features that are present in one image are not present in the other images.

(These shells were handled and characterized in a Class-100 clean room, but they were not made in a clean room.)

Submicrometer voids inside the shells' walls were characterized using the dark-field microscopy feature of the Leica DCM3D confocal microscope. The microscope was focused into the wall of a polystyrene shell at different depths (0.5-μm increments), and light-scattering features were observed at each of these discrete positions within the wall (Fig. 18). These features are presumed to result from vacuoles formed during the manufacturing process.

4. Conclusion

The highest-quality GDP targets produced to date possess up to several thousand domes, most with footprints smaller than 5 μm and heights smaller than 0.3 μm. These shells have too many defects to be suitable for high-yield implosions that are driven with low-adiabat laser pulses. Efforts to improve the surface quality of the shells by polishing them using the same protocol that is used for indirect-drive targets for the NIF had a marginal effect: the height of some of the larger domes was reduced, but many domes were unaffected by the polishing process and grooves and gouges were ground into the surface. Polishing may be a viable method for improving the quality of GDP shells sufficiently to meet the acceptance criteria for direct-drive experiments, but further development is needed.

The development of polystyrene shells for experiments on OMEGA began only recently (2016), and the progress that has been demonstrated so far is encouraging: the diameter and wall thickness of the shells is well controlled, although the

wall-thickness uniformity must be improved. A significant number of shells (up to 75%) from a production batch are rejected; because they have large cracks that form during the drying process; however, those shells are easily identified and rejected; this failure mode should be resolved with time. Similarly, scratches in the surface of the polystyrene shells that result from impact with the surface of the containers during the manufacture process should be eliminated as the fabrication process improves. The greater technical challenge is eliminating hundreds to thousands of voids in the wall of the polystyrene shells. The majority of the voids are smaller than 0.5 μm (in diameter) and are randomly distributed through the shell's wall. More problematic are those voids near the surface of the shell that either erupt into craters or create a dome-like swelling in the surface. These features are considerably fewer than the features that are present on GDP shells.

Properly characterizing targets for ICF experiments requires a combination of confocal, dark-field, scanning electron, and atomic force microscopy: Confocal microscopy provides height and spatial information of features on the surface that are larger than ~0.8 μm (footprint) and a target can be characterized using this method in one day using an automated system, which is an acceptable pace for identifying targets for implosion experiments; dark-field microscopy provides information about the number of features and how they are distributed throughout the wall of the shell and can be acquired rapidly; atomic force microscopy provides information about the shape and size of features over a wide size range (below 50-nm lateral sizes) but requires an unacceptably long time to fully characterize the shell's entire surface (>1 month); and, finally, electron microscopy provides a quick and accurate measurement of the lateral dimensions of features but requires extensive effort and time to provide height information.

Conflict of interest

None.

Acknowledgment

This material is based upon work supported by the Department of Energy National Nuclear Security Administration under Award Number DE-NA0001944, the University of Rochester, and the New York State Energy Research and Development Authority.

References

[1] S.P. Regan, V.N. Goncharov, I.V. Igumenshchev, T.C. Sangster, R. Betti, et al., Demonstration of fuel hot-spot pressure in excess of 50 Gbar for direct-drive, layered deuterium-tritium implosions on OMEGA, Phys. Rev. Lett. 117 (2016), https://doi.org/10.1103/PhysRevLett.117.025001, 025001; 117 (2016) 059903(E), https://doi.org/10.1103/PhysRevLett.117.059903.

[2] V.N. Goncharov, S.P. Regan, T.C. Sangster, R. Betti, T.R. Boehly, et al., Demonstrating ignition hydrodynamic equivalence in direct-drive cryogenic implosions on OMEGA, J. Phys. Conf. Ser. 717 (2016), https://doi.org/10.1088/1742-6596/717/1/012008, 012008.

[3] S.P. Regan, V.N. Goncharov, T.C. Sangster, E.M. Campbell, R. Betti, et al., The national direct-drive program: OMEGA to the national ignition facility, Fusion Sci. Technol. 73 (2018) 89, https://doi.org/10.1080/15361055.2017.1397487.

[4] B.W. McQuillan, A. Nikroo, D.A. Steinman, F.H. Elsner, D.G. Czechowicz, et al., The PAMS/GDP process for production of ICF target mandrels, Fusion Technol. 31 (1997) 381, https://doi.org/10.13182/FST31-381.

[5] M. Takagi, T. Norimatsu, T. Yamanaka, S. Nakai, Development of deuterated polystyrene shells for laser fusion by means of a density-matched emulsion method, J. Vac. Sci. Technol. A 9 (1991) 2145, https://doi.org/10.1116/1.577241.

[6] T. Bernat, C. Castro, A. Pasternak, J. Sin, O. Stein, et al., Quantitative submicron particulate characterization by dark-field microscopy, Fusion Sci. Technol. 73 (2017) 119, https://doi.org/10.1080/15361055.2017.1406236.

[7] Mountains® 7 Software, Digital Surf, 25000 Besançon France.

[8] ImageJ, http://rsbweb.nih.gov/ij/(27 January 2014).

[9] R.C. Cook, B.J. Kozioziemski, A. Nikroo, H.L. Wilkens, S. Bhandarkar, et al., National ignition facility target design and fabrication, laser part, Beams 26 (2008) 479, https://doi.org/10.1017/S0263034608000499.

[10] A. Nikroo, D. Woodhouse, Bounce coating induced domes on glow discharge polymer coated shells, Fusion Technol. 35 (1999) 202, https://doi.org/10.13182/FST99-A11963923.

[11] G. Wilemski, T. Boone, L. Cheung, D. Nelson, R. Cook, Prediction of phase separation during the drying of polymer shells, Fusion Technol. 28 (1995) 1773, https://doi.org/10.13182/FST95-A30411.